Dehydration of Na-jarosite, ferricopiapite, and rhomboclase at temperatures of 50 and 95°C: implications for Martian ferric sulfates

Yang Liu[a,b]* and Alian Wang[b]

Ferric sulfates with various hydration degrees were found on Mars by surface exploration and orbital remote sensing. The processes that they experienced during their formation and alteration relate to Martian hydrologic history and thus have been important topics for laboratory investigations. This study reports three sets of dehydration experiments conducted on Na-jarosite, ferricopiapite, and rhomboclase under two relative humidity conditions (5–6% RH and 10–11% RH) at two temperatures (50 and 95 °C), for which laser Raman spectroscopy and gravimetric measurements were the only two techniques used, *in situ* and non-invasively, to monitor the progress of these experiments. Our dehydration experiments show that OH-bearing Na-jarosite is relatively stable at 95 °C and RH < 11%, while H_2O/OH-bearing ferricopiapite and rhomboclase have converted almost entirely into anhydrous phases. These results have important applications on uncovering the mystery of rarely detected Martian ferric sulfates and on interpreting Mars remote sensing data. Copyright © 2015 John Wiley & Sons, Ltd.

Keywords: Raman spectroscopy; Mars; iron ferric sulfates; dehydration; remote sensing

Introduction

Sulfate is one of the two major types of secondary minerals, which records important past and present environmental conditions of the Mars surface and subsurface. Hydrated sulfates have been identified on Mars using orbital hyperspectral imaging data from the Observatoire pour la Minéralogie, l'Eau, les Glaces et l'Activité (OMEGA) onboard Mars Express and the Compact Reconnaissance Imaging Spectrometer for Mars (CRISM) onboard Mars Reconnaissance Orbiter.[1,2] Kieserite ($MgSO_4 \cdot H_2O$), polyhydrated sulfates ($MSO_4 \cdot nH_2O$, M = Mg, Fe, etc.) with unknown hydration degree, gypsum ($CaSO_4 \cdot 2H_2O$), and ferric sulfates (e.g. jarosite) are all identified.[3–9] By orbital remote sensing, Mg-sulfates and Ca-sulfates were found with wide distributions and large quantities on Mars. In contrast, Fe-sulfates have been observed only in localized areas, and the overall quantity is not comparable with other sulfates.

To date, the only unambiguous detection of ferric sulfates on Mars by both surface exploration and orbital remote sensing data is the identification of jarosite. In Meridiani Planum, jarosite [$KFe^{3+}(SO_4)_2(OH)_6$] was identified by the Mössbauer (MB) spectrometer on the Opportunity rover,[10] although new study shows similar MB spectral parameters from the solid solutions of jarosite-alunite.[11] Also, the visible and near infrared (VNIR) reflectance data acquired from CRISM explicitly revealed the presence of jarosite elsewhere on Mars.[8,9,12] Other than jarosite, an unidentified ferric-bearing phase termed 'Fe3D3' was observed in the MB spectra from the Opportunity rover,[13,14] which was potentially interpreted to be Fe(SO_4)(OH), schwertmannite ($Fe_{16}O_{16}(SO_4)_2$ $(OH)_{12} \cdot 10H_2O$), or super-paramagnetic hematite.[13–15] Also, OMEGA VNIR data indicate that schwertmannite is the likely mineral controlling spectral properties for Aram Chaos.[16] In Gusev Crater, the ferric-sulfate-rich soils named 'Paso Robles class of soils', which were excavated by the Spirit rover, are suggested to contain one or more of various ferric sulfates including ferricopiapite

($Fe^{3+}_{4.67}(SO_4)_6(OH)_2 \cdot 20H_2O$), rhomboclase ($HFe^{3+}(SO_4)_2 \cdot 4(H_2O)$), fibroferrite (Fe(OH)(SO_4) \cdot 5H_2O), and butlerite (Fe(OH)SO_4 \cdot 2H_2O).[17–19] Ferricopiapite was also potentially identified on Mars from orbit. For example, CRISM VNIR spectral features of the light-toned sulfate-bearing layered deposits in Juventae Chasma are most consistent with ferricopiapite, melanterite ($FeSO_4 \cdot 7H_2O$) or starkeyite ($MgSO_4 \cdot 4H_2O$), although a specific mineral cannot be uniquely identified.[19] More importantly, among the Paso Robles class of soils at Gusev, Tyrone salty soils demonstrated a two-layer structure (whitish and yellowish salty soil in upper and lower layers), on which the Pancam image and spectral analysis revealed a color change of the yellowish soil after its exposure to surface atmospheric conditions.[20] The spectral change in VNIR spectral range of this yellowish salty soil is consistent with the dehydration of ferricopiapite (the major component of Tyrone yellowish soil).[21,22]

The dehydration of ferric sulfates after exposure to Mars surface conditions is important to uncover the mystery of relatively rarely detected ferric sulfates on Mars surface by orbital remote sensing.

Similar to Mg-sulfates, Fe-sulfates display complex phase transitions as a function of relative humidity (RH) and temperature (T), and thus can serve as environmental indicators to past aqueous history on Mars. Furthermore, Fe-sulfates can present in neutral, acidic, and basic forms and thus imply more complicated environments. On Earth, Fe-sulfates often occur in acid mine drainages, where

---

* *Correspondence to: Yang Liu, Department of Civil and Environmental Engineering, University of Houston, Houston, TX, USA.*
E-mail: yliu97@uh.edu

a *The National Center for Airborne Laser Mapping, University of Houston, Houston, TX, USA*

b *Department of Earth and Planetary Sciences, Washington University in St. Louis, St. Louis, MO, USA*

acidic water outflows from metal mines and coal mines and the oxidation and dissolution of sulfide minerals and subsequent evaporation form various ferrous and ferric sulfates. Ferric sulfates represent a more advanced stage in the oxidation sequence and are often located further downstream from iron sulfide ores.[23] The presence of ferric sulfates is governed by additional variables such as pH and redox conditions, and thus records the past and present environmental conditions during their formation and alteration. Understanding precipitation conditions, the stability field, the phase transition pathways, and the reaction rates of phase transitions of ferric sulfates can greatly enhance the understanding of mission observations and Mars evolution. Laser Raman spectroscopy has been demonstrated to be an extremely powerful tool for *in situ* and non-invasive monitoring of the development of phase transitions of hydrous sulfates.[24–27]

The stability field and phase transition pathways of five hydrous ferric sulfates in the temperature range 50 to 5 °C have been studied that relate to Mars broad-scope environmental conditions in non-polar region.[28] The boundaries of deliquescence zone and the stability field in *T*-RH space were determined, and the experimental observations in ferricopiapite dehydration processes have provided a solid basis to interpret the observed spectral change of Fe-sulfate-rich Tyrone subsurface yellowish soils on Mars.[22] This research reports an experimental study on the dehydration of three ferric sulfates at a higher temperature range (50 and 95 °C), with a purpose to elucidate their dehydration products (and spectral characteristics) that might be produced by hydrothermal processes, post-volcanic, and post-impact events on Mars.

Experimental samples

The three ferric sulfates (Na-jarosite [$NaFe^{3+}_3(SO_4)_2(OH)_6$], ferricopiapite [$Fe^{3+}_{4.66}(SO_4)_6(OH)_2 \cdot 20(H_2O)$], and rhomboclase [$HFe^{3+}(SO_4)_2 \cdot 4(H_2O)$]) were used as the starting phases in the 12 dehydration experiments. They are selected because they have been either explicitly or potentially identified on Mars. Of the three ferric sulfates, ferricopiapite and rhomboclase were synthesized using the method described in the previous study,[29] and Na-jarosite was purchased from Rublev Colours. The chemical purity of synthesized hydrous ferric sulfates was ensured by the pure starting chemicals used in synthesis procedures. Their crystal structures were confirmed by X-ray diffraction (XRD) patterns (using PDF2006 database). Each starting ferric sulfate sample was reexamined by microbeam Raman spectroscopy in which over 100 Raman data points (diameter of ~6 μm) were collected from a flattened ferric sulfate powder sample placed on a glass slide. Consistent Raman spectral patterns and Raman peak positions were obtained from all 100 sampling spots in each of three starting ferric sulfates, thus confirming the homogeneity of each sample.

Dehydration experiments at two temperatures

The humidity buffer technology was used to drive the dehydration of ferric sulfates.[30,31] For these experiments, about 40–400 mg ferric sulfate powder was placed in a 12-mm-diameter straight-wall glass reaction vial. Each uncapped reaction vial was placed in a 25-mm-diameter straight-wall glass bottle that contains RH buffer (a binary salt plus its saturated aqueous solution[30,31]). The RH buffer bottle is capped tightly and sealed with Teflon tape. Note that the bottles were not vacuumed. Four experiments were conducted for each of the three starting ferric sulfates at two

temperatures (in 50 ± 1 and 95 ± 1 °C oven) and two RH buffers (RH = 5–6%, by saturated LiBr-H_2O solution and RH = 10–11%, by saturated LiCl-H_2O solution), respectively. The durations of these experiments are around 10 weeks (1680 h in total). During each experiment, 12 reaction vials were taken out from the buffer bottles after 5 weeks of dehydration and sealed immediately, to make gravimetric and laser Raman measurements to monitor the change in hydration degree and phase transitions, respectively. After these measurements, they were placed back into the buffer bottles to continue the dehydration. After 10 weeks of dehydration, gravimetric, laser Raman spectroscopy, and VNIR spectroscopy measurements were taken on the final dehydration products.

Phase identification at the intermediate and final stages of experiments

Laser Raman Spectroscopy (LRS) were taken on the initial ferric sulfate powder samples to confirm their homogeneity in hydration degree, and then on the intermediate and final dehydration products. The LRS measurements on dehydration products were taken through the glass wall of sealed reaction vials onto multiple spots at the sample surface to collect the Raman photons produced by the sample and to identify, non-invasively, the phase change that occurred during the dehydration process. The gravimetric measurements were taken at intermediate and final stages to monitor the loss of water in the mineral structure during the dehydration, and thus to confirm the phase identification made by LRS. For all of these measurements, the reaction vial was taken out from the buffer bottle and immediately capped; thus, no exchange between the sample powder and the laboratory atmospheric H_2O vapor occurred.

Raman spectra of the samples were obtained by a HoloLab5000-532 laser Raman spectrometer (Kaiser Optical Systems Inc.). A 20× microscopic objective (numerical aperture = 0.4) was used to focus the laser beam of 532 nm. Each measurement typically uses 2-s exposure time and 16 accumulations to obtain a Raman spectrum with good signal/noise ratio. Full range wavelength calibration and correction are made by using the emission lines of a Ne lamp. The laser line correction is made by using the Raman line (520.7 cm^{-1}) of a Si sample. The wavelength accuracy and precision were found to be better than 0.1 cm^{-1} in the spectral region of interest as determined by the spectral peak fitting using the GRAMS/AL software. To make gravimetric measurement, a Citizon® balance with resolution of 0.1 mg was used. The net mass loss of a sample in a reaction vial is calculated by subtracting the initial mass of powder sample from the mass of dehydration product, to derive the net loss of the number of H_2O per molecule. The VNIR spectra of the initial ferric sulfate powder samples and their dehydration products at the final stage were acquired in open laboratory condition, by an Analytical Spectral Devices FeildSpec3 spectrometer. The spectra cover a wavelength range of 0.35 to 2.5 μm with a 10-nm spectral resolution.

Structures and Raman and VNIR spectra of Na-jarosite, ferricopiapite, and rhomboclase

Structure and characteristic spectral feature of Na-jarosite

Jarosite is a Fe-rich end-member of the large jarosite-alunite supergroup of minerals. Jarosite can occur as an end-member of Na-jarosite, K-jarosite, and hydronium-jarosite and also as solid solutions among them.[32,33] Na-jarosite has a trigonal crystal structure, which consists of SO_4 tetrahedra and Fe cation in octahedral

sites with Na atoms in a dodecahedral site (Fig. 1(a)). Each Fe^{3+} cation is bonded to four OH and two SO_4 groups. The antisymmetric stretching vibration mode of SO_4 tetrahedra in Na-jarosite contributes doublet Raman peaks at 1109 and 1151 cm^{-1} (Fig. 2(b)).[34] In the hydroxyl stretching region, there is a sharp peak around 3388 cm^{-1} with a shoulder around 3362 cm^{-1} (Fig. 2(a)). In the VNIR spectral region, the absorption feature near 1.85 µm is due to the overtone of OH bending associated with SO_4 group, and the 2.265 µm band is due to combinational OH stretching and Fe–OH bending[35] (Fig. 3).

Structure and characteristic spectral feature of ferricopiapite

The crystal structure of ferricopiapite is shown in Fig. 1(b). There are 20 structural water molecules in a ferricopiapite formula unit that can be split into two types, coordinated to octahedra or loosely hydrogen bonded. Fourteen H_2O belong to type one that include six H_2O that surround Fe^{3+} to form $[Fe(OH_2)_6]$ octahedra, and eight H_2O are in two pairs of $[Fe(OH_2)_2(OH)O_3]$ octahedra with each pair interconnected by sharing a common hydroxyl (OH). Six H_2O belong to type two that are not part of any S-centered tetrahedra or Fe-centered octahedra but only linked to the framework by weak hydrogen bonding. Because ferricopiapite has both structural water

and hydroxyl, its Raman spectrum in this region shows two peaks 3523 and 3572 cm^{-1} due to OH stretching, sitting on the wing of a broad peak from the structural water (Fig. 2(a)). The intense
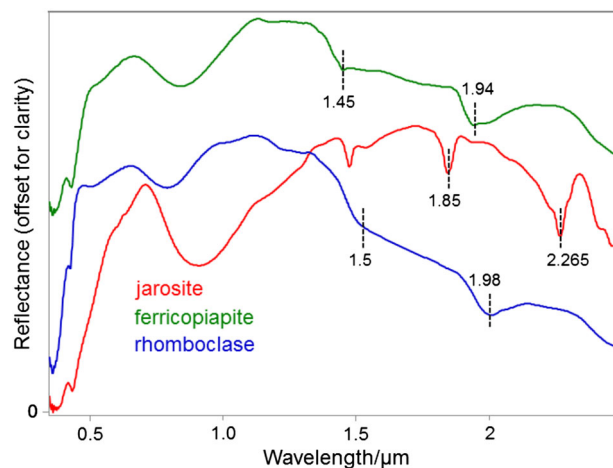

Figure 3. VNIR reflectance spectra of Na-jarosite, ferricopiapite, and rhomboclase. (This figure is available in colour online at wileyonlinelibrary.com/journal/jrs.)
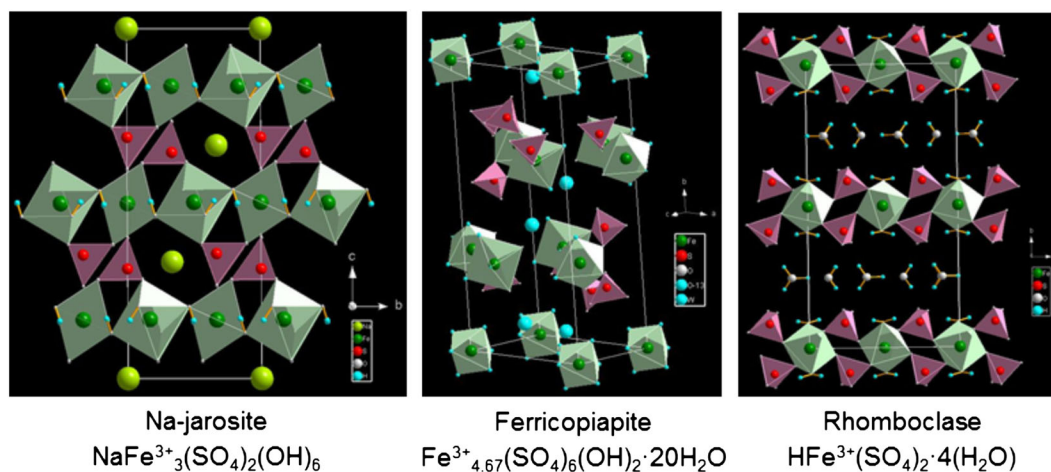

Figure 1. Crystal structures of (a) Na-jarosite, (b) ferricopiapite, and (c) rhomboclase. (This figure is available in colour online at wileyonlinelibrary.com/journal/jrs.)
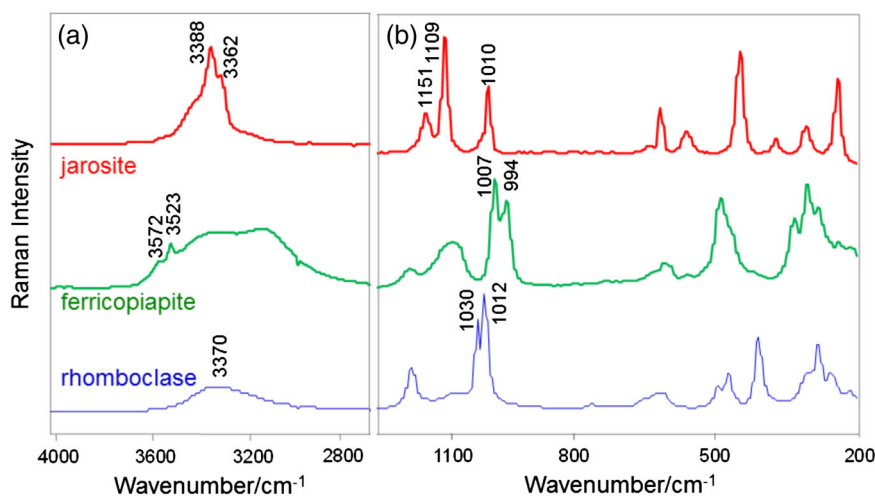

Figure 2. Raman spectra of Na-jarosite, ferricopiapite, and rhomboclase: (a) spectral range for H_2O/OH vibrational modes and (b) spectral range for fundamental modes of SO_4. (This figure is available in colour online at wileyonlinelibrary.com/journal/jrs.)

Raman peaks in the spectral region between 200 and 1200 cm^{-1} are due to SO_4 tetrahedra internal and external vibrations[22] (Fig. 2 (b)). In the VNIR spectral region, the absorption feature near 1.94 µm is due to H_2O combinational mode ($v_1 + v_2$) and 1.45 µm band is due to H_2O combinational mode ($v_1 + 2v_2$)[22] (Fig. 3).

Structure and characteristic spectral feature of rhomboclase

The rhomboclase crystal structure consists of parallel sheets with interconnected $FeO_4(H_2O)_2$ octahedra and SO_4 tetrahedra (Fig. 1(c)). In the sheets, each octahedron is linked to four S-centered tetrahedra, and each tetrahedron links two Fe-centered octahedra.[36] Similar to ferricopiapite, rhomboclase also has two types of structure waters. The two vertices of the $FeO_4(H_2O)_2$ octahedron that are not bonded to a sulfate tetrahedron are occupied by H_2O molecules. $H_5O_2^+$ ions occur between the sheets and bond the rhomboclase structure with hydrogen bonding. The broad Raman peaks in the 3200–3400 cm^{-1} spectral region are due to the combination of the symmetric stretching, the weaker antisymmetric stretching, and the overtone of the bending vibrational modes of structural water (Fig. 2(a)). Similar to ferricopiapite, there are intense Raman peaks in the spectral region between 200 and 1200 cm^{-1}, which are due to SO_4 tetrahedra internal and external vibrations[22] (Fig. 2(b)). Rhomboclase has a similar spectral shape with ferricopiapite in the VNIR wavelength region, but the water bands at 1.4 and 1.9 µm are shifted to the longer wavelengths[22] (Fig. 3).

Results of the dehydration experiments

The dehydration process of hydrous salts is affected by the environmental parameters such as T and RH as well as the crystal structure, stability field, phase transition pathway, and activation energy of the salt. The standard Raman spectra based on which the phase identifications were made have been published by previous studies.[22,29]

Results of gravimetric measurements

The results from gravimetric measurements of three sets of experiments at two temperatures and two RH buffers are plotted in Fig. 4(a–c). The balance (Mettler PM480 Delta Range) used for gravimetric measurements has an uncertainty of ±1 mg. The mass ranges we used in this study are ~400 mg for Na-jarosite, ~50 mg for ferricopiapite, and ~250 mg for rhomboclase, and thus, the uncertainty in calculating the number of structural H_2O/OH held by these molecules based on the gravimetric measurement uncertainty was about ±0.1 OH for jarosite, ±1 H_2O for ferricopiapite, and ±0.1 H_2O for rhomboclase.

Figure 4 reveals very different dehydration pathways among Na-jarosite, ferricopiapite, and rhomboclase during the first 5 weeks. The dehydration of these samples became very slow after 5 weeks, and the level of hydration was maintained for the rest period of the dehydration experiments. Figure 4(a) shows that Na-jarosite maintains almost all of the structural OH in these experiments. At 50 °C, Na-jarosite lost ~0.1 OH per molecule and ~0.2 OH at a much higher temperature 95 °C after 10 weeks of dehydration. Very differently, at 50 °C, ferricopiapite lost 2 H_2O/OH per molecule at an RH of 10–11% and 5 H_2O/OH at a lower RH (5–6%). At 95 °C, ferricopiapite lost as many as 16 structural H_2O/OH per molecule at an RH of 10–11% and all of the structural H_2O/OH at 5–6% RH (Fig. 4(b)). The stepwise loss of the structural water in ferricopiapite is consistent with two types of H_2O in its crystal structure, where six
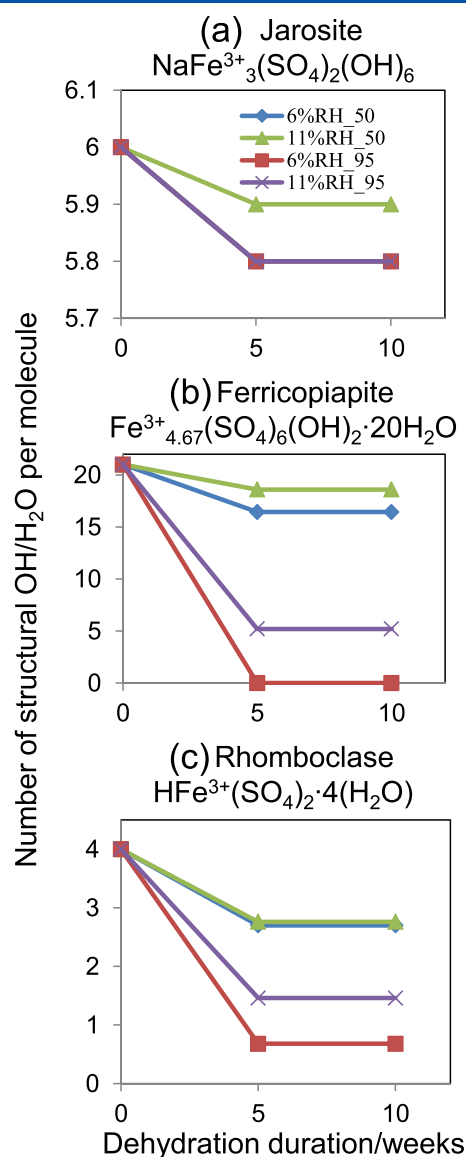

Figure 4. Number of H_2O per molecule *versus* experimental duration in weeks, during the process of dehydration under two temperatures and two relative humidity, calculated based on gravimetric measurements: (a) Na-jarosite, (b) ferricopiapite, and (c) rhomboclase. (This figure is available in colour online at wileyonlinelibrary.com/journal/jrs.)

hydrogen-bonded structural waters are expected to be easily lost during the dehydration, while the other 14 H_2O molecules (building blocks of Fe-centered octahedra) would be lost with more difficulty. The dehydration of rhomboclase has a similar trend as ferricopiapite. At 50 °C, the hydration degree reached ~2.7–2.8 H_2O/OH per molecule at the two RH buffers. At 95 °C, it lost more waters and maintained ~1.5 H_2O per molecule at 10–11% RH and ~0.7 H_2O per molecule at 5–6% RH (Fig. 4(c)).

These experimental results reveal that, first, Na-jarosite is relatively stable even at relatively high temperatures and low RH. This is also consistent with previous stability studies on jarosite. For example, Babcan indicated that jarosite stability zone is between pH 1 and 3 at 20 and 200 °C.[37] The dynamic heating experiments conducted by Dutrizac and Jambor showed that jarosite will not decompose during heating until a temperature of 400 °C is reached.[38] Secondly, the dehydration of ferricopiapite and rhomboclase is strongly dependent on temperatures, and also on

RH. Thirdly, the stepwise dehydration processes of ferricopiapite and rhomboclase match very well with their structural features, i.e. the bonding strength of two types of H_2O molecules. The actual molecular phase changes during the dehydration are revealed by laser Raman spectroscopy and VNIR spectroscopy, which are discussed in the following sections.

Results of LRS measurements

Laser Raman Spectroscopy (LRS) measurements were taken on 12 reaction vials from dehydration experiments of Na-jarosite, ferricopiapite, and rhomboclase at the intermediate (5 weeks) and final stages (10 weeks). Based on gravimetric measurements, the dehydrations of all three samples have almost all stopped at 5 weeks. The phase identifications made by non-invasive laser Raman measurements indicate that there are no phase changes between the two time stages, and the summary of the phase identification results is shown in Table 1. Thus, here, we only show the Raman spectra (and the VNIR spectra in the next section) of the dehydration products after 10 weeks.

The Raman spectra of the dehydration products of Na-jarosite, ferricopiapite, and rhomboclase are shown in Fig. 5(a–c), and the phase identifications are shown in Table 1. All of the dehydration products of Na-jarosite have *loss of peak details* (marked as LOPD in Table 1) in OH vibrational region (Fig. 5(a)). The intensity of the Raman peak at $3362\,cm^{-1}$ has gradually reduced and finally disappeared in the spectra of the dehydration products. In the SO_4 fundamental vibrational region, peaks at 1109 and $1010\,cm^{-1}$ show small downshift (marked by dotted lines in Fig. 5(a)). The changes in these spectral features imply a slight structural distortion without a large reduction of the hydration degree. There is no new phase produced during the dehydration.

At 50 °C and 5–11% RH, ferricopiapite dehydrated into a different structure, *quasi-Am*, as reported by previous studies,[28] that can maintain a variable 14–19 structural H_2O per molecule. Comparing with ferricopiapite, quasi-Am has an obvious reduction of peak intensity at $3400\,cm^{-1}$ (Fig. 5(b)). Based on ferricopiapite crystal structure (Fig. 1(b)), we believe that the water molecules lost during this experiment stage were the six, interstitial, hydrogen-bonded H_2O molecules. At 95 °C, the dehydration of ferricopiapite developed further: It converted totally into a dehydrated form $Fe(OH)SO_4$ in fibroferrite-butlerite group at 6% RH after 5 weeks. This phase has distinct Raman patterns featured with a sharp peak at $3348\,cm^{-1}$ in the water vibrational region and three peaks at 1060, 1101, and $1184\,cm^{-1}$ in the SO_4 vibrational region (Fig. 5(b)). In these cases,

the H_2O molecules that are the building blocks of $[Fe(OH_2)_6]$ and $[FeO_3(OH)(OH_2)_2]$ octahedra disappeared.

The dehydration of rhomboclase under 50 °C and 11% RH appeared as the intensity reduction of H_2O Raman peak at $3364\,cm^{-1}$, and the *loss of peak details* (LOPD) of its fundamental modes ($1300–900\,cm^{-1}$) (Fig. 5c), which signify the onset of structural change. Under higher T (95 °C, 6% and 11% RH) or lower RH (6%) at 50 °C, rhomboclase converted to an anhydrous crystalline phase that has a different structure from mikasaite ($Fe_2(SO_4)_3$). This phase has a distinct XRD pattern that did not show as a match in the XRD database PDF2009 and consequently was named temporally as UK 19.[28] The Raman spectra show that the double peaks at 1012 and $1030\,cm^{-1}$ have shifted to a shorter wavelength region and become a single sharp peak at $1058\,cm^{-1}$ (Fig. 5(c)). The flat Raman spectrum in $4000–2800\,cm^{-1}$ (bottom spectrum in Fig. 5(c)) shows that it is anhydrous.

Results of VNIR spectral characters

The comparison between the VNIR spectra of Na-jarosite, ferricopiapite, and rhomboclase and their dehydration products is shown in Fig. 6(a–c). Consistent with Raman identifications and very minor gravimetric changes, there is no significant change of the OH spectral features of Na-jarosite, suggesting very low degree of dehydration (Fig. 6(a)). Note that, in the shorter wavelength region, there are subtle shortward wavelength shift of iron absorption feature at ~0.9 μm and decreasing of the slope from 0.4 to 0.7 μm.

Quasi-Am (Fig. 6(b)) has a very similar spectral pattern to ferricopiapite, except slight increasing of the slope from 0.43 to 0.5 μm and longward wavelength shift of iron absorption feature at ~0.85 μm. This observation suggests that the loss of the hydrogen-bonded structural waters has only subtle distortion of the crystal structure and thus no significant change in the VNIR spectra. The dehydration product of ferricopiapite at high T, $Fe(OH)SO_4$, has a distinct VNIR spectral pattern, with almost no absorption near 1.9 μm but a sharp absorption band at ~2.235 μm due to metal-OH vibration. In this case, the loss of most 14 H_2O molecules as building blocks of Fe-centered octahedra causes large change of the crystal structure from ferricopiapite to $Fe(OH)SO_4$.

The VNIR spectra of the dehydration products of rhomboclase at 50 °C show no significant change compared with the original samples (Fig. 6(c)). The spectra of the high-T dehydration product of rhomboclase, anhydrous UK 19,[28] have no structural H_2O-related and OH-related VNIR absorption features observed, which is consistent with Raman identification, as an anhydrous phase of ferric sulfates.

Table 1. Summary of phase identifications from laser Raman spectroscopy

		Temperature (°C) 50		Temperature (°C) 95	
Relative humidity	Week	11.1%	5.5%	10.1%	5.3%
Jarosite	5	LOPD, v_3 shift	LOPD	LOPD, v_3 shift	LOPD
	10	LOPD, v_3 shift	LOPD, v_3 shift	LOPD, v_3 shift	LOPD, v_3 shift
Ferricopiapite	5	Quasi-Am[a]	Quasi-Am	Quasi-Am + $Fe(OH)SO_4$	Quasi-Am + $Fe(OH)SO_4$
	10	Quasi-Am	Quasi-Am	Quasi-Am + $Fe(OH)SO_4$	$Fe(OH)SO_4$
Rhomboclase	5	I_{H_2O} ↓, LOPD	4w + UK 19[b]	UK 19	UK 19
	10	I_{H_2O} ↓, LOPD	4w + UK 19	UK 19	UK 19

LOPD, lost of peak detail.
[a]Quasi-Am, ferricopiapite lost some of six hydrogen-bonded H_2O and has 19–14 H_2O and slightly distorted structure, UK 9.[28]
[b]UK 19, anhydrous ferric sulfate, with no XRD matching (not mikasaite).[28]
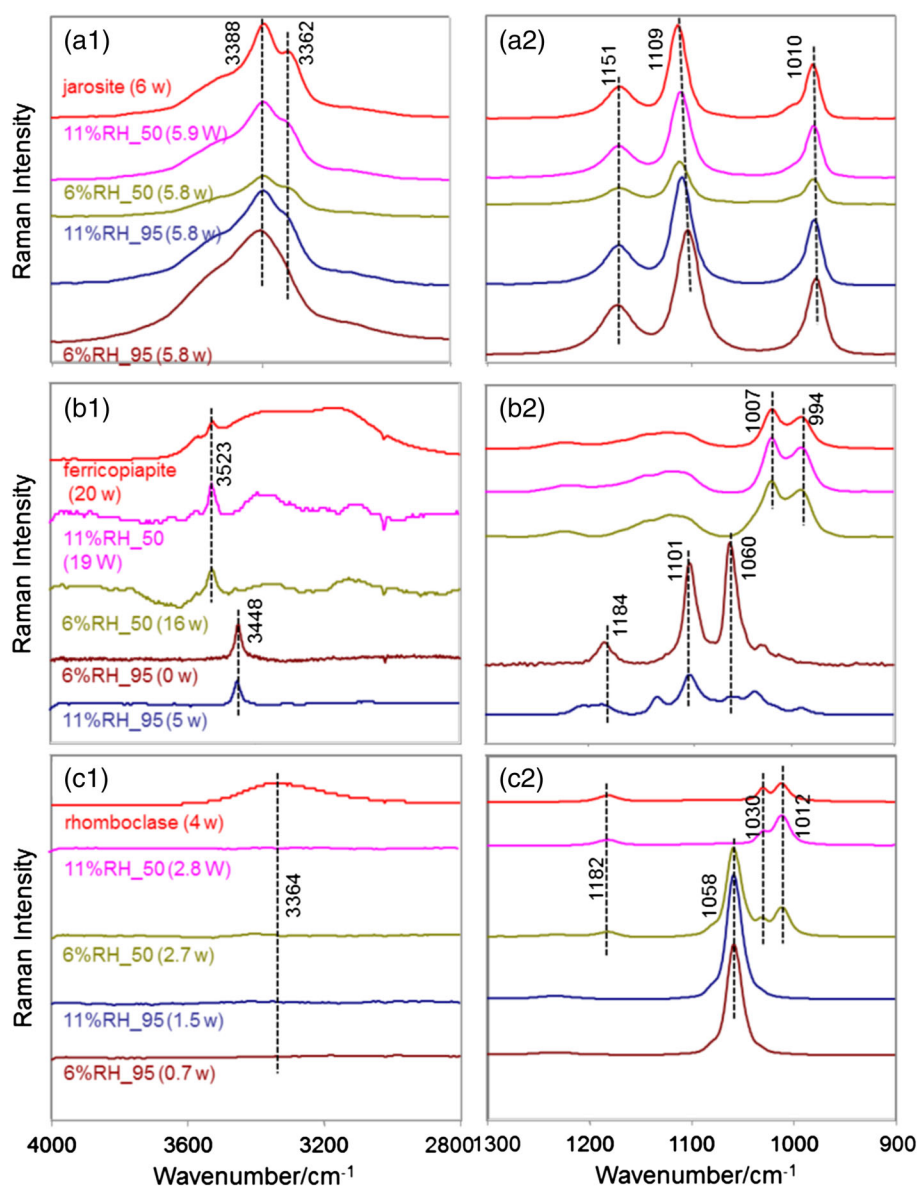
Figure 5. (a) Raman spectra of dehydration products of Na-jarosite at two temperatures (50 and 95 °C) and two relative humidity (6% and 11%): (a1) spectral range for H₂O/OH vibrational modes and (a2) spectral range for fundamental modes of SO₄. (b) Raman spectra of dehydration products of ferricopiapite at two temperatures (50 and 95 °C) and two relative humidity (6% and 11%): (b1) spectral range for H₂O/OH vibrational modes and (b2) spectral range for fundamental modes of SO₄. (c) Raman spectra of dehydration products of rhomboclase at two temperatures (50 and 95 °C) and two relative humidity (6% and 11%): (c1) spectral range for H₂O/OH vibrational modes and (c2) spectral range for fundamental modes of SO₄. (This figure is available in colour online at wileyonlinelibrary.com/journal/jrs.)

The comparison of VNIR spectra of the original ferric sulfates samples and their dehydration products at 50 and 95 °C is important for the interpretation of Mars remote sensing observations.

Implications on Martian ferric sulfates

Data from Mars OMEGA and CRISM spectrometers have provided numerous information of Martian surface mineralogy. Minerals present on Mars can be identified using the diagnostic absorption features in their VNIR spectral region, and one direct way to interpret these spectral data is to compare them with the spectral library of the terrestrial materials for most cases. However, not all OMEGA or CRISM data can find appropriate matches in the general spectral library. Thus, laboratory experiments such as dehydration experiments can provide additional potential spectral library to aid the

remote sensing data interpretation. Ferric sulfates have been identified in localized areas on Mars. The dehydration experiments show that the dehydration processes of ferric sulfates that occurred either under Mars' current condition[28] or at high temperatures (this study) can cause changes in their spectral characteristics, which may obscure the identification of these original ferric sulfates on Mars. Of the three samples that we studied, both ferricopiapite and rhomboclase show spectral changes due to the distortion of their crystal structure at 50 °C during dehydration or the new phases generated at 95 °C, which were identified by laser Raman spectroscopy data analysis. One possible implication of our dehydration experimental results is that, if on Mars, ferricopiapite and rhomboclase were found (i.e. Paso Robles class of salty soils at Gusev), the location may not have experienced a $T > 95$ °C for a long period. However, future laboratory work is needed to test this conclusion by considering other factors, such as a very different
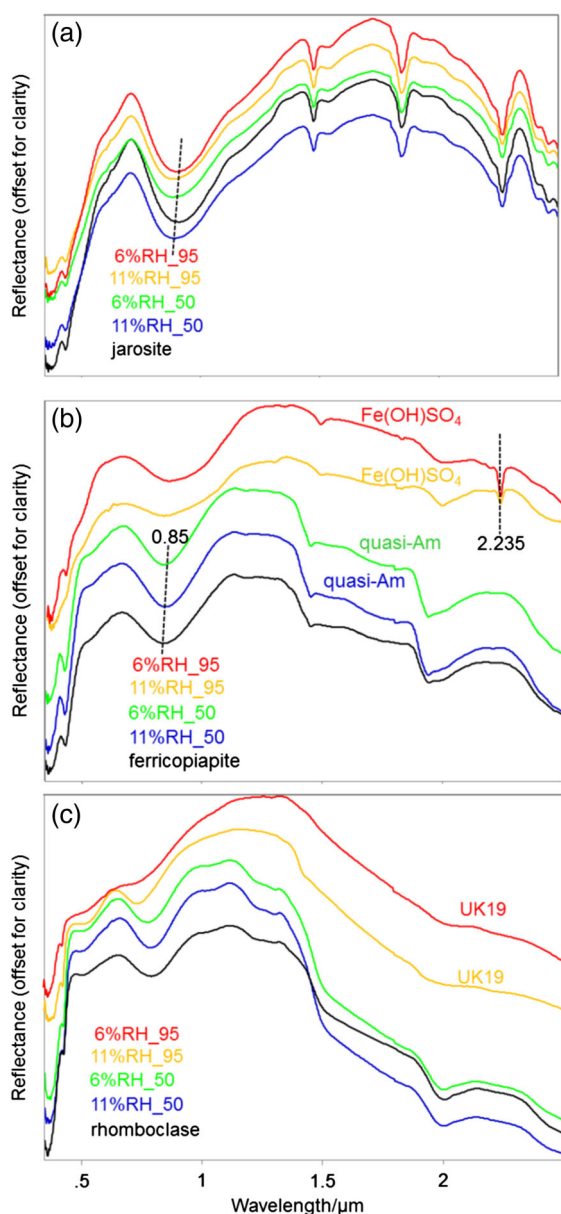
Figure 6. (a) VNIR reflectance spectra of dehydration products of Na-jarosite. The spectra are vertically shifted in order to show the changes in spectral characteristics during the dehydration. (b) VNIR reflectance spectra of dehydration products of ferricopiapite. The spectra are vertically shifted in order to show the changes in spectral characteristics during the dehydration. (c) VNIR reflectance spectra of dehydration products of rhomboclase. The spectra are vertically shifted in order to show the changes in the spectral characteristics during the dehydration. (This figure is available in colour online at wileyonlinelibrary.com/journal/jrs.)

Mars environmental condition from the Earth (i.e. low pressure) and potentials mixtures of ferricopiapite and rhomboclase with other clay minerals, which may substantially influence the stability of ferricopiapite and rhomboclase on Mars.

In our dehydration experiment, Na-jarosite maintained almost all the structural OH at a temperature as high as 95 °C and very low humidity condition (5–6% RH). On Mars, jarosite is the most abundant ferric sulfate that has been identified by orbital remote sensing and has a relatively wide distribution (e.g. in Melas Chasma, in Marth Vallis, and on the plains surrounding the Valles Marineris). Jarosite in these areas may be direct products from weathering processes and may have been preserved, even in the areas where they reside
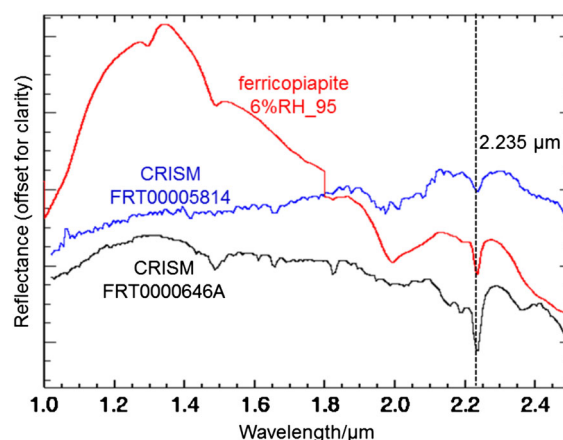

Figure 7. Comparison of VNIR spectra of the dehydration product of ferricopiapite (at 95 °C and a relative humidity of 6%) and the spectra obtained by CRISM from two locations on Mars. The unique absorption band at 2.35 μm is a characteristic VNIR feature of Fe(OH)SO$_4$. (This figure is available in colour online at wileyonlinelibrary.com/journal/jrs.)

have been through high temperature conditions such as hydrothermal processes, post-volcanism, and post-impact mechanisms, as indicated by our dehydration experiments.

Furthermore, VNIR spectral features of Fe(OH)SO$_4$ were obtained by CRISM on Mars, as shown in Fig. 7, where the black-labeled and blue-labeled spectra are from Aram Chaos[39] and Juventae Chasma,[19] respectively, and the red-labeled spectrum is the dehydration product of ferricopiapite at 95 °C and 6% RH conditions. The CRISM spectra have a distinct absorption feature at 2.235 μm that is not consistent with any minerals in the CRISM spectral library. However, the dehydration product Fe(OH)SO$_4$ from ferricopiapite shows a similar absorption feature at 2.235 μm that indicates the presence of these dehydration products in these areas. Note that the formation of Fe(OH)SO$_4$ in our experiments through heating of ferricopiapite at 95 °C and low RH level is quite different from previously reported formation paths of Fe(OH)SO$_4$, i.e. by heating melanterite (FeSO$_4\cdot$7H$_2$O) at 50 °C and vacuum desiccation[40,41] or by heating at a much higher temperature (240 °C).[39] Our experiment result provides an alternative interpretation of the observed remote sensing data. This further indicates that ferricopiapite might have been formed in the two areas originally and then dehydrated into Fe(OH)SO$_4$ during heating processes such as hydrothermal, post-volcanic, and post-impact events on Mars.

References

[1] J. P. Bibring, A. Soufflot, M. Berthé, Y. Langevin, B. Gondet, P. Drossart, M. Bouyé, M. Combes, P. Puget, A. Semery, G. Bellucci, V. Formisano, V. Moroz, V. Kottsov, G. Bonello, S. Erard, O. Forni, A. Gendrin, N. Manaud, F. Poulet, G. Poulleau, T. Encrenaz, T. Fouchet, R. Melchiorri, F. Altieri, N. Ignatiev, D. Titov, L. Zasova, A. Coradini, F. Capacionni, P. Cerroni, S. Fonti, N. Mangold, P. Pinet, B. Schmitt, C. Sotin, E. Hauber, H. Hoffmann, R. Jaumann, U. Keller, R. E. Arvidson, J. F. Mustard, F. Forget, *Eur. Space Agency Spec. Publ.* **2004**, ESA SP-1240, 37–49.

[2] S. Murchie, R. Arvidson, P. Bedini, K. Beisser, J. P. Bibring, J. Bishop, J. Boldt, P. Cavender, T. Choo, R. T. Clancy, E. H. Darlington, D. D. Marais, R. Espiritu, D. Fort, R. Green, E. Guinness, J. Hayes, C. Hash, K. Heffernan, J. Hemmler, G. Heyler, D. Humm, J. Hutcheson, N. Izenberg, R. Lee, J. Lees, D. Lohr, E. Malaret, T. Martin, J. A. McGovern, P. McGuire, R. Morris, J. Mustard, S. Pelkey, E. Rhodes, M. Robinson, T. Roush, E. Schaefer, G. Seagrave, F. Seelos, P. Silverglate, S. Slavney, M. Smith, W. J. Shyong, K. Strohbehn, H. Taylor, P. Thompson, B. Tossman, M. Wirzburger, M. Wolff, *J. Geophys. Res. Planets* **2007**, *112*, E05S03.

[3] R. E. Arvidson, F. Poulet, J. P. Bibring, M. J. Wolff, A. Gendrin, R. V. Morris, J. J. Freeman, Y. Langevin, N. Mangold, G. Bellucci, *Science* **2005**, *307*, 1576.

[4] J. P. Bibring, Y. Langevin, A. Gendrin, B. Gondet, F. Poulet, M. Berthe, A. Soufflot, R. Arvidson, N. Mangold, J. Mustard, P. Drossart, *Science* **2005**, *307*, 1576.

[5] A. Gendrin, N. Mangold, J. P. Bibring, Y. Langevin, B. Gondet, F. Poulet, G. Bonello, C. Quantin, J. F. Mustard, R. E. Arvidson, S. LeMouelic, *Science* **2005**, *307*, 158.

[6] Y. Langevin, F. Poulet, J. P. Bibring, B. Gondet, *Science* **2005**, *305*, 1584.

[7] S. L. Murchie, J. F. Mustard, B. L. Ehlmann, R. E. Milliken, J. L. Bishop, N. K. McKeown, E. Z. Noe-Dobrea, F. P. Seelos, D. L. Buczkowski, S. M. Wiseman, R. E. Arvidson, J. J. Wray, G. Swayze, R. N. Clark, D. J. D. Marais, A. S. McEwen, J. P. Bibring, *J. Geophys. Res. Planets* **2009**, *114*, E00D06.

[8] R. E. Milliken, G. A. Swayze, R. E. Arvidson, J. L. Bishop, R. N. Clark, B. L. Ehlmann, R. O. Green, J. P. Grotzinger, R. V. Morris, S. L. Murchie, J. F. Mustard, C. Weitz, *Geology* **2008**, *36*, 847.

[9] W. H. Farrand, T. D. Glotch, J. W. Rice Jr., J. A. Hurowitz, G. A. Swayze *Icarus* **2009**, *204*, 478.

[10] G. Klingelhöfer, R. V. Morris, B. Bernhardt, C. Schroder, D. S. Rodionov, P. A. de Souza, A. Yen, R. Gellert, E. N. Evlanov, B. Zubkov, J. Foh, U. Bonnes, E. Kankeleit, P. Gutlich, D. W. Ming, F. Renz, T. Wdowiak, S. W. Squyres, R. E. Arvidson, *Science* **2004**, *306*, 1740.

[11] T. M. McCollom, B. L. Ehlmann, A. Wang, B. M. Hynek, B. Moskowitz, T. S. Berquó, *Am. Mineral.* **2014**, *99*, 948.

[12] Y. Liu, R. E. Arvidson, R. Li, W. Wang, Lunar and Planetary Science Conference XLIII, *19–23 March 2012*, **2012**, http://www.lpi.usra.edu/meetings/lpsc2012/pdf/2572.pdf, 2572.

[13] B. C. Clark, R. V. Morris, S. M. McLennan, R. Gellert, B. J. Jolliff, A. H. Knoll, S. W. Squyres, T. K. Lowenstein, D. W. Ming, N. J. Tosca, A. Yen, P. R. Christensen, S. Gorevan, J. Bruckner, W. Calvin, G. Dreibus, W. Farrand, G. Klingelhoefer, H. Waenke, J. Zipfel, J. F. Bell, J. Grotzinger, H. Y. McSween, R. Rieder, *Earth Planet. Sci. Lett.* **2005**, *240*, 73.

[14] R. V. Morris, G. Klingelhöfer, C. Schröder, D. S. Rodionov, A. Yen, D. W. Ming, P. A. de Souza Jr, T. Wdowiak, I. Fleischer, R. Gellert, B. Bernhardt, U. Bonnes, B. Cohen, E. N. Evlanov, J. Foh, P. Gutlich, E. Kankeleit, T. McCoy, D. Mittlefehldt, F. Renz, M. Schmidt, B. Zubkov, S. Squyres, R. Arvidson, *J. Geophys. Res. Planets* **2006**, *111*, E12S15.

[15] W. H. Farrand, J. F. Bell III, J. R. Johnson, B. L. Jolliff, A. H. Knoll, S. M. McLennan, S. W. Squyres, W. M. Calvin, J. P. Grotzinger, R. V. Morris, J. Soderblom, S. D. Thompson, W. A. Watters, A. S. Yen, *J. Geophys. Res. Planets.* **2007**, *112*, E05S02.

[16] Y. Liu, R. E. Arvidson, M. J. Wolff, M. T. Mellon, J. G. Catalano, A. Wang, J. L. Bishop, *J. Geophys. Res. Planets* **2012**, *117*, E00J11.

[17] R. E. Arvidson, S. W. Ruff, R. V. Morris, D. W. Ming, L. S. Crumpler, A. S. Yen, S. W. Squyres, R. J. Sullivan, J. F. Bell III, N. A. Cabrol, B. C. Clark, W. H. Farrand, R. Gellert, R. Greenberger, J. A. Grant, E. A. Guinness, K. E. Herkenhoff, J. A. Hurowitz, J. R. Johnson, G. Klingelhöfer, K. W. Lewis, R. Li, T. J. McCoy, J. Moersch, H. Y. McSween, S. L. Murchie, M. Schmidt, C. Schröder, A. Wang, S. Wiseman, M. B. Madsen, W. Goetz, S. M. McLennan, *J. Geophys. Res. Planets* **2008**, *113*, E12S33.

[18] R. V. Morris, G. Klingelhofer, C. Schroder, I. Fleischer, D. W. Ming, A. S. Yen, R. Gellert, R. E. Arvidson, D. S. Rodionov, L. S. Crumpler, B. C. Clark, B. A. Cohen, T. J. McCoy, D. W. Mittlefehldt, M. E. Schmidt, P. A. de Souza Jr, S. W. Squyres, *J. Geophys. Res. Planets* **2008**, *113*, E12S42.

[19] J. L. Bishop, M. Parente, C. M. Weitz, E. Z. N. Dobrea, L. H. Roach, S. L. Murchie, P. C. McGuire, N. K. McKeown, C. M. Rossi, A. J. Brown, W. M. Calvin, R. Milliken, J. F. Mustard, *J. Geophys. Res. Planets* **2009**, *114*, E00D09.

[20] A. Wang, J. F. Bell III, R. Li, J. R. Johnson, W. Farrand, E. A. Cloutis, R. E. Arvidson, L. Crumpler, S. W. Squyres, S. M. McLennan, K. Herkenhoff, S. W. Ruff, A. T. Knudson, W. Chen, R. Greenberger, the Athena Science Team, *J. Geophys. Res. Planets* **2008**, *113*, E12S40.

[21] J. R. Johnson, J. F. Bell, E. Cloutis, M. Staid, W. H. Farrand, T. Mccoy, M. Rice, A. Wang, A. Yen, *J. Geophys. Res. Planets* **2007**, *34*, L13202.

[22] A. Wang, Z. Ling, *J. Geophys. Res. Planets* **2011**, *116*, E00F17.

[23] J. I. Jambor, D. K. Nordstrom, C. N. Alpers, *Rev. Mineral. Geochem.* **2000**, *40*, 305.

[24] A. Wang, J. F. Freeman, B. L. Jolliff, I. M. Chou, *Geochim. Cosmochim. Acta* **2006**, *70*, 6118.

[25] A. Wang, J. J. Freeman, B. L. Jolliff, *J. Geophys. Res. Planets* **2009**, *114*, E4.

[26] A. Wang, J. J. Freeman, I. M. Chou, B. L. Jolliff, *J. Geophys. Res. Planets* **2011**, *116*, E12006.

[27] A. Wang, C. F. William, M. T. Michael, M. Zheng, *Icarus* **2013**, *226*, 980.

[28] A. Wang, Z. Ling, J. J. Freeman, *Icarus* **2012**, *218*, 622.

[29] Z. Ling, A. Wang, *Icarus* **2010**, *209*, 422.

[30] L. Greenspan, *J. Res. Natl. Bur. Stand.* **1977**, *81A*, 89.

[31] I. M. Chou, R. R. Seal II, B. S. Hemingway, *Am. Mineral.* **2002**, *87*, 108.

[32] P. Bayliss, U. Kolitsch, E. H. Nickel, A. Pring, *Mineral. Mag.* **2010**, *74*, 919.

[33] S. J. Mills, F. Hatert, E. H. Nickel, G. Ferraris, *Eur. J. Mineral.* **2009**, *21*, 1073.

[34] O. T. K. Sasaki, H. Konno, *Can. Mineral.* **1998**, *36*, 1225.

[35] J. L. Bishop, E. Murad, *Am. Mineral.* **2005**, *90*, 1100.

[36] R. C. Peterson, E. Valyashko, R. Wang, *Can. Mineral.* **2009**, *47*, 625.

[37] J. Babcan, *Goel Zb.* **1971**, *22*, 299.

[38] J. E. Dutrizac, J. L. Jambor, *Rev. Mineral. Geochem.* **2000**, *40*, 405.

[39] K. A. Lichtenberg, R. E. Arvidson, R. V. Morris, S. L. Murchie, J. L. Bishop, T. D. Glotch, E. Noe Dobrea, J. F. Mustard, J. Andrews-Hanna, L. H. Roach, *J. Geophys. Res. Planets* **2010**, *115*, E00D17.

[40] K. Connor, A. Wang, 11th GeoRaman International Conference, *15–19 June 2014*, **2014**, http://www.hou.usra.edu/meetings/georaman2014/pdf/5008.pdf, 5008.

[41] A. Wang, Y. Zhou, *Icarus.* **2014**, *234*, 162.